


Research Article

Development and Evaluation of a Novel Polymer Drug Delivery System Using Cromolyn-Polyamides-Disulfide using Response Surface Design

Nadeen Mohammad Alkurdi,¹ Samer Hasan Hussein-Al-Ali ^{1,2} Awad Albalwi,³ Mike Kh. Haddad,⁴ Yousef Aldalahmed,¹ and Dalia Khalil Ali^{1,5}

¹Department of Basic Pharmaceutical Sciences, Faculty of Pharmacy, Isra University, Amman 11622, Jordan

²Department of Chemistry, Faculty of Science, Isra University, Amman 11622, Jordan

³Department of Chemistry, College of Science, King Saud University, Riyadh, Saudi Arabia

⁴Department of Renewable Energy Engineering, Faculty of Engineering, Isra University, P.O. Box 22, Amman 11622, Jordan

⁵Department of Physiotherapy, Faculty of Allied Medical Sciences, Isra University, Amman 11622, Jordan

Correspondence should be addressed to Samer Hasan Hussein-Al-Ali; sameralali72@yahoo.com

Received 23 February 2022; Accepted 30 May 2022; Published 28 June 2022

Academic Editor: Ranjit De

Copyright © 2022 Nadeen Mohammad Alkurdi et al. This is an open access article distributed under the Creative Commons Attribution License, which permits unrestricted use, distribution, and reproduction in any medium, provided the original work is properly cited.

The aim of this study was to employ nanoparticles as drug carriers. The research involved the design of cromolyn polyamide-disulfide nanocomposites to overcome the problem of frequent cromolyn doses and improve their properties. The cromolyn polyamide-disulfide samples were prepared using several amounts of cromolyn and sodium polyamide-disulfide polymer at different pH values. Analysis of variance (ANOVA) was performed to obtain the significant independent variables affecting the dependent response by using a *P* value lower than 0.05. The nanocomposites produced were characterized using Fourier transform infrared (FTIR) spectroscopy and *in vitro* release. An FTIR test was used to evaluate the functional groups of cromolyn in nanocomposites, which indicated that the drug was encapsulated inside the polymer. All data indicated the presence of cromolyn in the nanocomposites. The release profile of nanocomposites was found to be sustained. Therefore, the outcome of this research project could be a starting point for further work to optimize and assess polyamide-disulfide polymers for delivering another drug.

1. Introduction

Nanoparticles are a broad category of materials that include particulate substances with dimensions less than 100 nm. Nanoparticles are categorized into different groups based on their shapes, properties, and size and offer various advantages [1, 2], including sustained release in the gastrointestinal tract, GIT, better penetration, and excellent uptake by cells [3, 4]. Furthermore, these nanoparticles are biodegradable and nontoxic to cells. All these benefits enable them to be ideal candidates with improved effectiveness. There are several advantages of using nanoparticles in drug delivery, including improved stability *in vivo*, as well as long-term

capacity for release and penetration through small capillaries and body compartments [3].

Nanoparticles may also improve drug bioavailability and enhance biodistribution properties and pharmacokinetics. The following are the primary criteria for nanoparticle delivery: high loading capacity, slow dissociation *in vivo*, and optimized targeting to the desired tissue with reduced absorption by other tissues. The production of formulations that have these characteristics, while being cost-effective and simple to design, is important for the development of an effective delivery system [5].

Polyamides and disulfide polymers were synthesized by interfacial polycondensation of diamines and cystine amino

acids with dicarbonyl dichlorides derived from renewable dicarboxylic acids [6].

Cromolyn was initially used to treat allergic asthma and soon has been shown to be successful in treating intestinal allergies, mastocytes, and allergic skin conditions. The mast cell stabilizer is widely used for its therapeutic function in the treatment of allergic diseases [7]. Cromolyn sodium is synthesized by linking two monochrome nuclei with a shared alkyl residue. It is unique in its mechanism of action and wide range of clinical applications, although cromolyn sodium has been approved for the treatment of asthma since 1973. It is a white, hydrated powder that is lipophobic and highly polar, and its highly ionized acid salt has a PKa of 2 [8]. Cromolyn can be administered via inhalation or through intranasal, oral, or ophthalmic routes [9]. Under the biopharmaceutical classification scheme, cromolyn is classified as a Class III compound (BCS). Cromolyn's high solubility and poor permeability make it difficult to absorb from the gastrointestinal tract. Two carboxyl groups make cromolyn very hydrophilic, hampering its absorption across the gastrointestinal tract (GIT) and resulting in poor bioavailability in the treatment of health issues [10].

We expect the drug to reach its location at a certain concentration and be sustained for a long time for effective treatment; however, the drug's effect can be limited by several factors, including drug destruction. As a result, studies are being conducted on how to enhance the drug reaction and analyze its association with other cells as well as its inability to penetrate tissues because of its chemical character. Some researchers have attempted to improve the drug response by adding polymers with various physicochemical properties [11, 12].

Our study aims to devise a simple method to obtain a safe, stable mucoadhesive nanoparticulate formulation that can retain cromolyn inside the nasal mucosa. The nanocomposites were characterized in terms of particle size, zeta potential, and %LE. Furthermore, in vitro release studies were performed to study the nanoparticles' ability to deliver the drug in the nasal cavity.

2. Materials and Methods

2.1. Materials. The following chemicals were obtained from commercial sources and used: cromolyn from Sigma, polysulfide polyamine polymer from Dr. Dalia, sodium hydroxide from Chem Co (England), phosphate-buffered saline solution, ferric chloride of 98% purity, and deionized water.

2.2. Preparation of Blank-Polymer Nanoparticles and Cromolyn-Polymer Nanocomposites. The modified method, called the inotropic gelation method, was used for the preparation of nanoparticles and nanocomposites [13, 14]. A solution of cromolyn, FeCl₃, was prepared in distilled water, and a polymer solution was prepared in 0.1 Molar of NaOH. The solution of cromolyn was mixed with the polymer solution. After that, the solution of FeCl₃ was added dropwise to the mixture of the drug and polymer under stirring, and the pH was adjusted to 4.4 and 2.2. The nanocomposites were stirred overnight to allow the formation of nanocomposites with uniform size. The nanocomposites were collected using centrifugation (11,000 rpm). The final product was washed three times using distilled water and dried to obtain the final dry powder.

2.3. Methodology

2.3.1. Modeling of Different Responses. In this study, we studied the effect of different independent variables (drug, FeCl₃, polymer concentrations, and pH value) on three responses. The %LE is the first response that was used as a parameter and is defined as the total amount of entrapped drug divided by the total weight of nanoparticles. Particle size and zeta potential were the second and third responses used in this study.

2.3.2. Full Factorial Design (FFD). According to the levels in Table 1 and the full factorial design in Table 2, 54 samples were prepared according to Minitab 18 software [15, 16].

2.3.3. Multiple Regression Method. Regression analysis was used to show a mathematical relationship between the responses (%LE, particle size, and zeta potential) and independent variables (cromolyn, polymer, FeCl₃, and pH) [17].

2.4. Determination of the %LE of Cromolyn. %LE of cromolyn in the prepared nanocomposites was measured using an ultracentrifugation system at 11000 rpm, and the absorbance for free drug in the supernatant was measured at λ_{\max} of 326 nm using the following equation [18]:

$$\% \text{loading} = \frac{\text{total mass of cromolyn} - \text{total mass of free cromolyn}}{\text{mass of nanocomposites}} \times 100. \quad (1)$$

2.5. Determination of Particle Size and Zeta Potential. At 25°C, each sample was analyzed in triplicate. The samples were dispersed in distilled water for 15 minutes, and they were sonicated. The cuvette was filled and covered. The

Malvern logo should be directed to the instrument front and the absence of bubbles in the cuvette should be checked. The software automatically defined the run numbers in each measurement.

TABLE 1: Levels of drug, FeCl₃, polymer, and pH factors.

Factor	Unit	Low level	Middle level	High level
Drug	gm	0.05	0.10	0.20
FeCl ₃	gm	0.3	0.6	1.2
polymer	gm	0.05	0.10	0.20
pH	None	2.2	—	4.4

2.6. *In Vitro Release Study of Cromolyn from Nanocomposites.* The in vitro release of cromolyn from the nanocomposites was determined in PBS at pH 7.4 using a Perkin Elmer UV-vis spectrophotometer with λ_{\max} of 326 nm. Suitable amount of nanocomposite was added to release media. The percentage release of cromolyn in PBS was obtained using the following equation [19]:

$$\% \text{release} = \frac{\text{mass of cromolyn at time } t}{\text{mass of cromolyn in nanocomposite}} \times 100. \quad (2)$$

2.7. *Instrumentation.* UV-vis spectra were measured to determine the release of cromolyn using a Shimadzu UV-1601 spectrophotometer. Fourier transform infrared (FTIR) spectroscopy spectra of the materials were recorded over the range of 400–4000 cm⁻¹ on a Perkin Elmer spectrometer (model Smart UAIR-two). The zeta potential was measured at 25°C by dynamic light scattering (DLS) using a Malvern Zetasizer Nano ZS (Malvern Instruments, Malvern, UK). X-ray diffraction (XRD) technique was used in the range of 5–70° by XRD D5005 diffractometer with CuK α radiation (Siemens, Munich, Germany). Scanning electron microscopy (FE-SEM) was done using Zeiss LEO 1550 (Jena, Germany).

3. Results and Discussion

3.1. *Multiple Linear Regression Analysis Using Full Quadratic.* The result values of the three models are shown in Table 3. The *R*-squared, *R*-sq (adj), and *R*-sq (pred) values for %LE are 94.95%, 93.32%, and 90.48%, respectively. The difference between *R*² and adjusted *R*² was 2.84%, which showed a good result for the data.

Additionally, from Table 3, the *R*-squared, *R*-sq (adj), and *R*-sq (pred) values for zeta potential are 93.69%, 91.43%, and 87.10%, respectively. The difference between *R*² and adjusted *R*² was 4.33%, which showed a good result for the data.

After taking the source (liner and 2-way interaction) during data analysis, the software was used to build the equation for %LE and zeta potential models. Table 4 shows the equations for the %LE and zeta potential models.

3.2. ANOVA for %LE, Size, and Zeta Potential

3.2.1. *ANOVA for %LE.* Table 5 shows the ANOVA data analysis for %LE models. From the table, the linear interaction contains drug, FeCl₃, polymer, and PH, while the 2-way interaction contains six different ways (drug*FeCl₃, drug*polymer, drug*PH, FeCl₃*polymer, FeCl₃*PH, and

TABLE 2: Matrix for full factorial design.

Run order	Drug (gm)	FeCl ₃ (gm)	Polymer (gm)	PH
1	0.05	0.6	0.05	2.2
2	0.05	0.6	0.20	4.4
3	0.05	0.3	0.10	4.4
4	0.20	0.3	0.10	2.2
5	0.05	0.3	0.05	4.4
6	0.10	0.6	0.10	2.2
7	0.20	1.2	0.20	2.2
8	0.05	1.2	0.20	2.2
9	0.20	0.3	0.20	4.4
10	0.10	0.3	0.20	4.4
11	0.05	0.3	0.10	2.2
12	0.20	1.2	0.05	2.2
13	0.20	0.6	0.10	2.2
14	0.10	0.3	0.10	4.4
15	0.10	1.2	0.20	4.4
16	0.10	0.6	0.20	4.4
17	0.20	0.6	0.20	2.2
18	0.20	1.2	0.10	4.4
19	0.10	0.6	0.20	2.2
20	0.05	0.3	0.05	2.2
21	0.10	1.2	0.10	2.2
22	0.05	0.6	0.05	4.4
23	0.05	0.6	0.10	2.2
24	0.05	0.6	0.10	4.4
25	0.05	1.2	0.20	4.4
26	0.20	0.3	0.20	2.2
27	0.20	1.2	0.10	2.2
28	0.20	1.2	0.05	4.4
29	0.10	1.2	0.05	2.2
30	0.20	0.6	0.05	2.2
31	0.05	0.3	0.20	2.2
32	0.05	1.2	0.10	2.2
33	0.20	0.6	0.20	4.4
34	0.10	0.3	0.05	4.4
35	0.10	1.2	0.05	4.4
36	0.10	0.3	0.05	2.2
37	0.20	0.6	0.10	4.4
38	0.20	0.3	0.10	4.4
39	0.20	1.2	0.20	4.4
40	0.10	0.3	0.10	2.2
41	0.20	0.3	0.05	4.4
42	0.10	1.2	0.20	2.2
43	0.10	0.6	0.02	4.4
44	0.05	0.3	0.20	4.4
45	0.10	1.2	0.10	4.4
46	0.05	0.6	0.20	2.2
47	0.10	0.6	0.05	2.2
48	0.10	0.3	0.20	2.2
49	0.05	1.2	0.05	4.4
50	0.20	0.3	0.05	2.2
51	0.05	1.2	0.10	4.4
52	0.10	0.6	0.10	4.4
53	0.20	0.6	0.05	4.4
54	0.05	1.2	0.05	2.2

polymer*PH). With further analysis of the data, we found that only PH as linear (drug*PH, FeCl₃*PH, and polymer*PH) had a *P* value greater than 0.05 and nonsignificant properties, while the other sources had significant properties.

TABLE 3: Regression model for dependent variables.

	R-sq (pred)	R-sq (adj)	R-sq
90.48%	93.32%	94.95%	%LE
87.10%	91.43%	93.69%	Zeta potential

TABLE 4: The %LE and zeta potential equations.

%LE	=	0.58 + 327.7 drug + 3.66 FeCl ₃ + 6.0 polymer + 0.17 pH -202.6 drug*FeCl ₃ -570 drug*polymer + 14.20 drug*pH + 92.8 FeCl ₃ *polymer -1.99 FeCl ₃ *pH -11.41 polymer*pH
Zeta potential	=	67.8 + 144.1 drug -56.5 FeCl ₃ + 127.0 polymer -22.88 pH + 42.0 drug*FeCl ₃ -233 drug*polymer -48.1 drug*pH -13.4 FeCl ₃ *polymer + 25.78 FeCl ₃ *pH -30.6 polymer*pH

TABLE 5: ANOVA data of LE.

Source	DF	Adj SS	Adj MS	F value	T value	VIF	P value
Model	10	6173.26	617.33	58.25	—	—	0.001
Linear	4	3771.58	942.89	88.97	—	—	0.001
Drug	1	2819.09	2819.09	266.00	16.31	1.20	0.001
FeCl ₃	1	1162.33	1162.33	109.67	-10.47	1.34	0.001
Polymer	1	125.90	125.90	11.88	-3.45	1.31	0.002
pH	1	39.15	39.15	3.69	-1.92	1.22	0.064
2-Way interaction	6	1200.79	200.13	18.88	—	—	0.001
Drug*FeCl ₃	1	755.44	755.44	71.28	-8.44	1.16	0.001
Drug*polymer	1	131.92	131.92	12.45	-3.53	1.43	0.001
Drug*pH	1	33.43	33.43	3.15	1.78	1.18	0.086
FeCl ₃ *polymer	1	139.76	139.76	13.19	3.63	1.22	0.001
FeCl ₃ *pH	1	24.20	24.20	2.28	-1.51	1.11	0.141
Polymer*pH	1	21.16	21.16	2.00	-1.41	1.11	0.168
Error	31	328.54	10.60	—	—	—	—
Total	41	6501.81	—	—	—	—	—

3.2.2. ANOVA for Zeta Potential. Table 6 shows the ANOVA data analysis for the zeta potential models. From the table, the linear interaction contains drug, FeCl₃, polymer, and PH, while the 2-way interaction contains six different ways (drug*FeCl₃, drug*polymer, drug*PH, FeCl₃*polymer, FeCl₃*PH, and polymer*PH). With further analysis of the data, we found that only FeCl₃ and PH as linear (drug*PH and FeCl₃*PH) had *P* values less than 0.05 and significant properties.

3.2.3. ANOVA for Particle Size. Table 7 shows the ANOVA data analysis for particle size models. From the table, the linear model contains drug, FeCl₃, polymer, and PH, while the 2-way interaction contains six different ways (drug*FeCl₃, drug*polymer, drug*PH, FeCl₃*polymer, FeCl₃*PH, and polymer*PH). With further analysis of the data, we found that the *P* value for the particle size model was nonsignificant (0.339 > 0.05), so the particle size model was removed from the work.

3.3. Evaluation of the Models

3.3.1. Pareto Chart of Responses Standardized Effect and Half Normal Plot of the Standardized Effects. A Pareto chart in Figure 1 is a graphical overview of the process factors and/or interactions of influence, in ranking order from the most

influencing to the least influencing. A threshold line (*P* value 0.05) indicates the minimum magnitude of statistically significant effects. The insignificance of factors can also be reasserted from the half normal plot (Figures 2(a) and 2(b)), where the points that do not fall near the fitted line and the variables that have a small effect on the output response are usually centered around zero. The effect of A (cromolyn) has the highest standardized effect on %LE, followed by B, AB, BC, AC, and C. All the significances of the factors are shown in the half normal plot (Figure 1(a)).

Figure 1(b) shows that PH, FeCl₃, FeCl₃*PH, and drug*PH passed the reference line at 2.05, which means that these factors greatly affect the zeta potential at the 0.05 level. Additionally, this plot made it clear that zeta potential was not highly dependent on polymer*PH, drug*FeCl₃, drug*polymer, polymer, drug, and FeCl₃*polymer. The effect of D (PH) has the highest standardized effect on the zeta potential, followed by B, B, and AD. All the significances of the factors are shown in the half normal plot (Figure 1(b)).

From the results shown in Figure 1(c) and for the Pareto charts of particle size, it can be seen that the particle size was not significant for all factors.

3.3.2. Residual Plots for %LE and Zeta Potential. The normality of the data can be checked by the normal probability plot of the residual, high value of *R*², and approximate straight line of the normal probability plot, as presented in

TABLE 6: ANOVA results for zeta potential.

Source	DF	Adj SS	Adj MS	F value	T value	VIF	P value
Model	10	20062.1	2006.21	41.56	—	—	0.001
Linear	4	14610.4	3652.61	75.66	—	—	0.001
Drug	1	17.4	17.39	0.36	-0.60	1.31	0.553
FeCl ₃	1	4322.6	4322.60	89.54	9.46	1.31	0.001
Polymer	1	19.3	19.26	0.40	-0.63	1.40	0.533
pH	1	6514.6	6514.65	134.95	-11.62	1.23	0.001
2-Way interaction	6	4517.6	752.94	15.60	—	—	0.001
Drug*FeCl ₃	1	29.8	29.81	0.62	0.79	1.33	0.439
Drug*polymer	1	26.9	26.88	0.56	-0.75	1.27	0.462
Drug*pH	1	333.7	333.74	6.91	-2.63	1.22	0.014
FeCl ₃ *polymer	1	3.3	3.30	0.07	-0.26	1.19	0.796
FeCl ₃ *pH	1	3209.4	3209.43	66.48	8.15	1.38	0.001
Polymer*pH	1	123.5	123.54	2.56	-1.60	1.42	0.121
Error	28	1351.7	48.28	—	—	—	—
Total	38	21413.8	—	—	—	—	—

TABLE 7: ANOVA data of particle size.

Source	DF	Adj SS	Adj MS	T value	VIF	P value
Model	10	66952	6695.2	—	—	0.339
Linear	4	33543	8385.9	—	—	0.231
Drug	1	1041	1040.8	-0.43	1.14	0.672
FeCl ₃	1	16719	16718.9	1.71	1.08	0.095
Polymer	1	1768	1768.1	0.56	1.17	0.581
pH	1	11510	11509.9	-1.42	1.11	0.164
2-Way interaction	6	26922	4487.0	—	—	0.585
Drug*FeCl ₃	1	3082	3082.2	0.74	1.06	0.467
Drug*polymer	1	49	48.8	0.09	1.18	0.927
Drug*pH	1	1391	1391.4	-0.49	1.09	0.624
FeCl ₃ *polymer	1	16810	16809.9	-1.72	1.09	0.095
FeCl ₃ *pH	1	208	208.3	-0.19	1.04	0.849
Polymer*pH	1	3677	3677.4	-0.80	1.11	0.427
Error	35	199300	5694.3	—	—	—
Total	45	266252	—	—	—	—

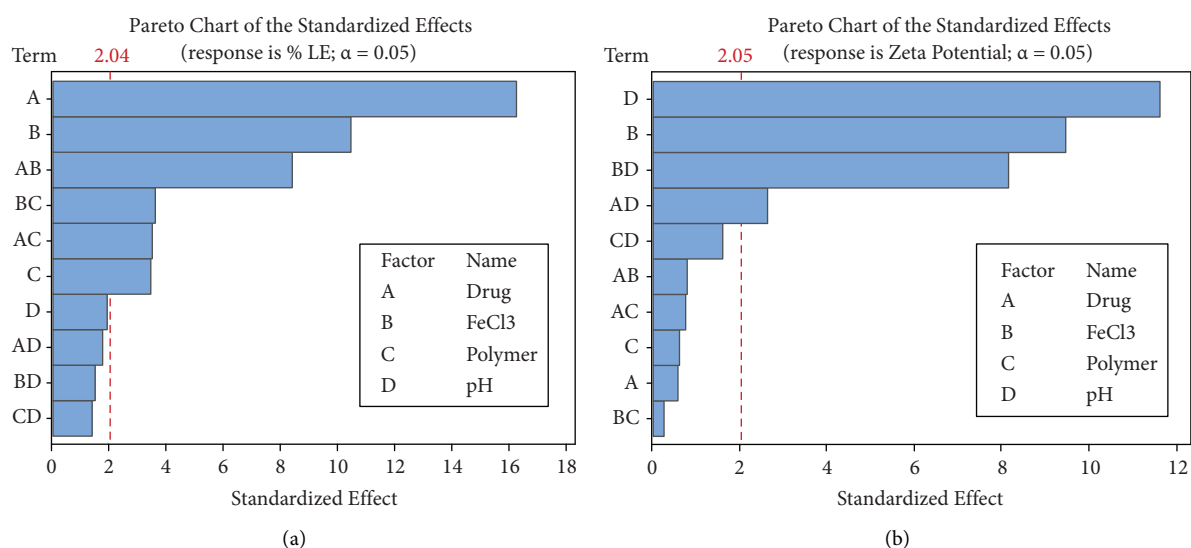
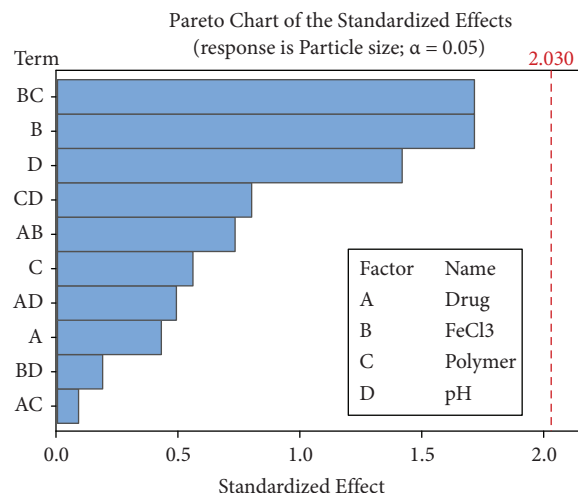
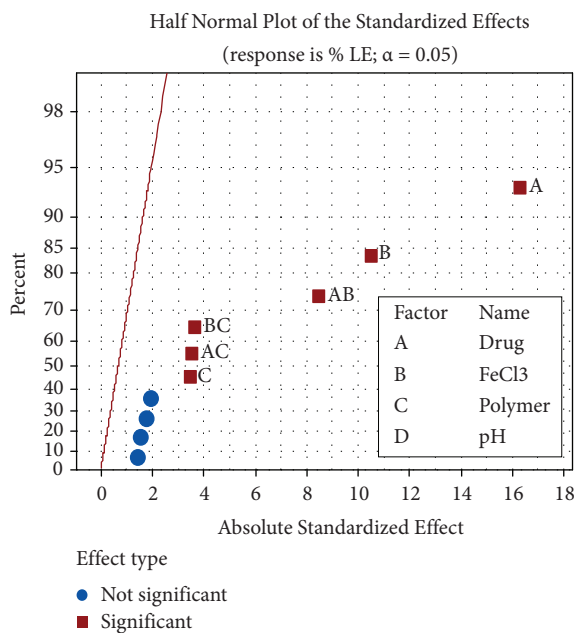


FIGURE 1: Continued.

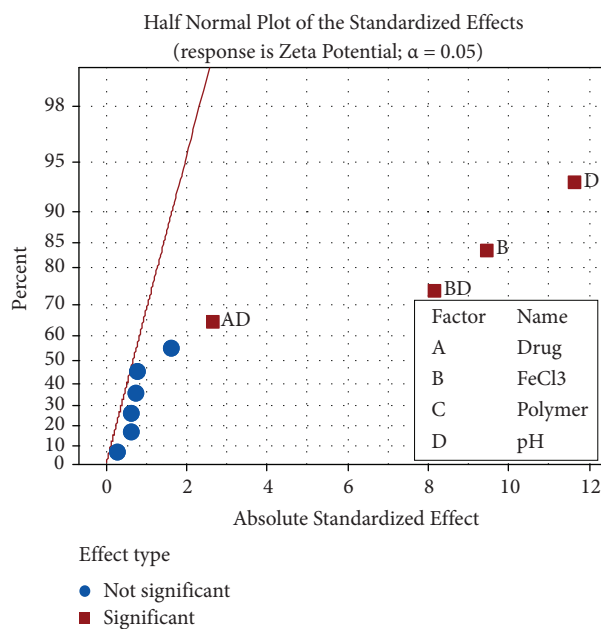


(c)

FIGURE 1: Pareto chart of the standardized effects on %LE (a), zeta potential (b), and particle size (c).



(a)



(b)

FIGURE 2: Half normal plot for %LE (a) and zeta potential (b).

Figure 3(a) and Figure 4(a) for %LE and zeta potential, respectively. The plot of this figure is normally distributed and resembles a straight line. There was no evidence of nonnormality and any pointing to possible outliers. Figures 3(b) and 4(b) were observed to be within the acceptable ranges, and the histogram showed a visibly bell-shaped pattern of normal distribution.

Figures 3(c) and 4(c) clarify the residuals versus the fits plot, and Figures 3(d) and 4(d) explain the residuals versus the order plot for the %LE and zeta potential to validate the model in which residues are not dependent on each other, using a residual value versus arrangement chart. The residuals on the plot should ideally fall randomly around the centerline. The

residuals were used to validate the model in which the residuals are randomly distributed and have a constant variance in the versus fits plot. Ideally, points must fall randomly on both sides. In general, these results showed that the experiment does not contain any possibility of systemic errors.

3.3.3. Contour Plot and Surface Plot of %LE and Zeta Potential against Selected Independent Variables. Figure 5(a) shows the surface plot of %LE, where the independent variables are drug and FeCl₃. From the figure, the highest %LE (>45%) can be collected at a high level of drug (>0.175 gm) and a low level of FeCl₃ (<0.49 gm) with a fixed

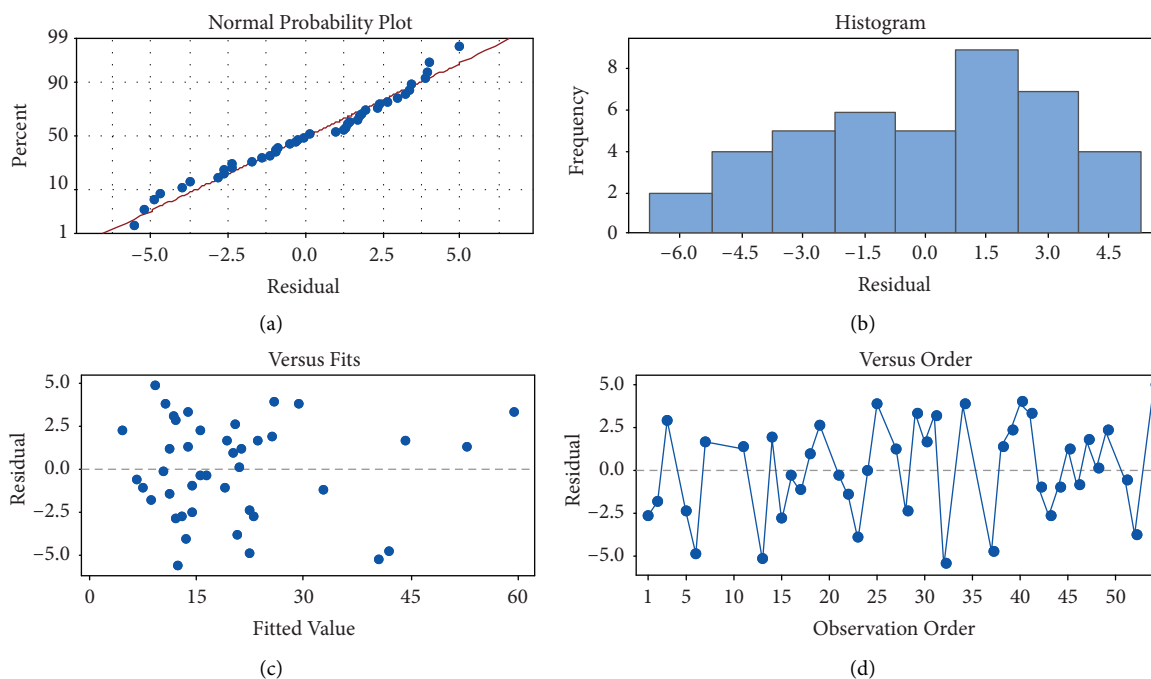


FIGURE 3: Residual plot for %LE. (a) Normal probability plot; (b) histogram; (c) versus fits; (d) versus order.

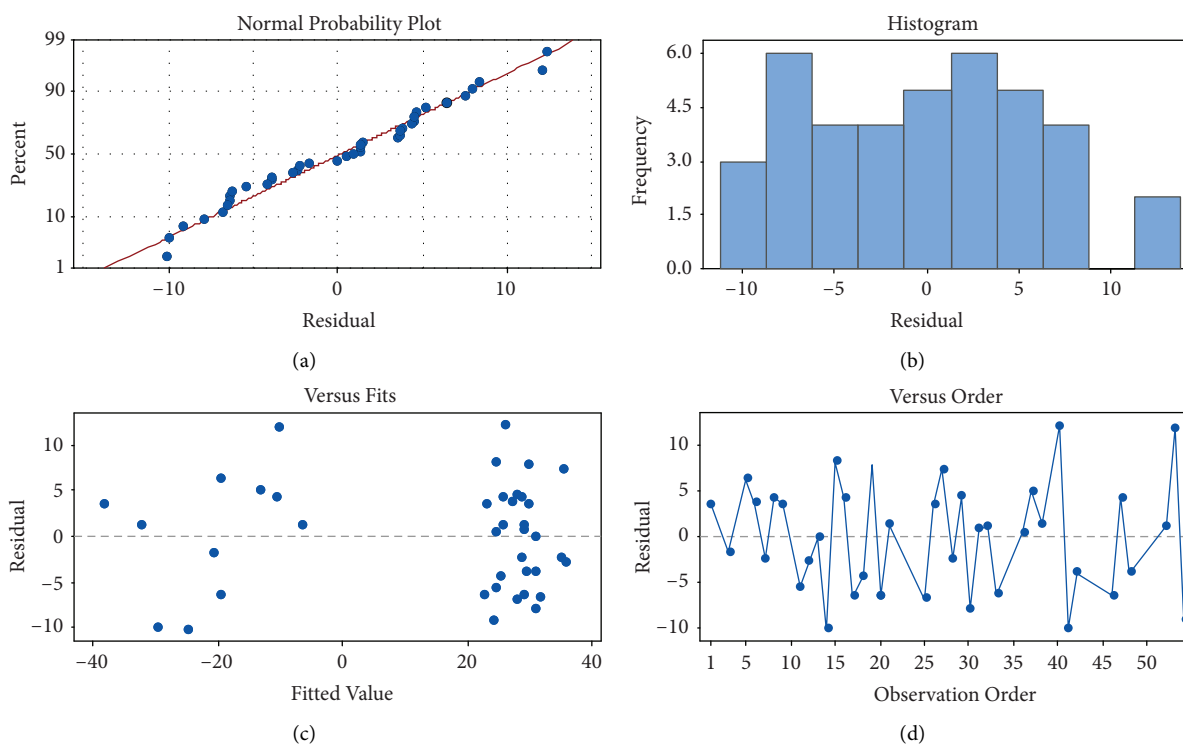


FIGURE 4: Residual plot for zeta potential. (a) Normal probability plot; (b) histogram; (c) versus fits; (d) versus order.

value of polymer (0.125 gm) and pH at 3.3 gm. These results are also shown in the contour plot in Figure 5(b).

From Figure 5(c) of the surface plot and Figure 5(d) of the contour plot of %LE, the %LE with more than 30% can be collected at a high level of drug (0.2 gm) with a large range in

pH starting from 2.2 to 4.4, with a fixed value of FeCl_3 (0.75 gm) and polymer (0.12 gm).

The effect of the polymer and drug on the %LE is shown in Figures 5(e) and 5(f). The results show that a %LE greater than 35% can be collected by using a concentration greater

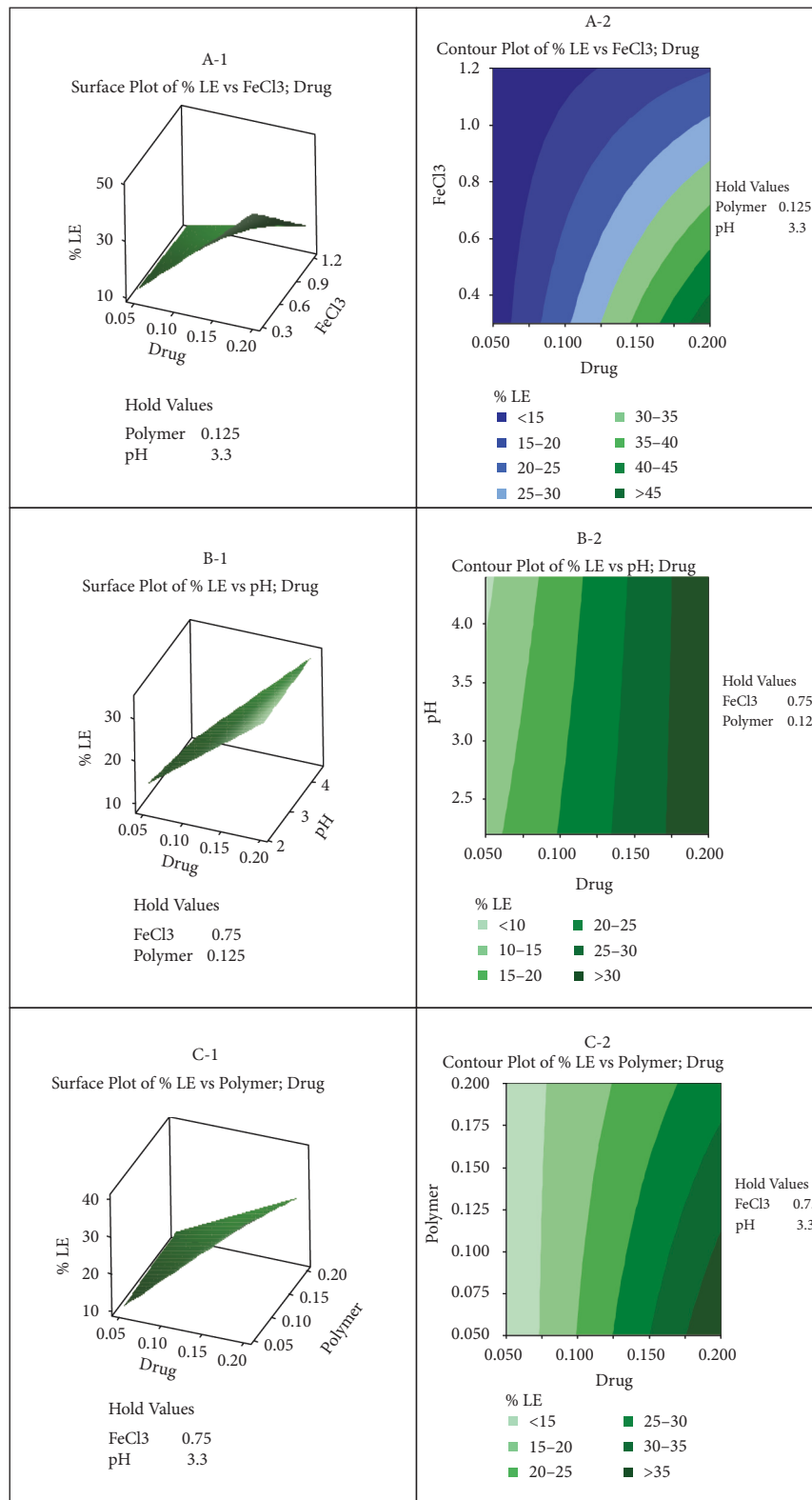


FIGURE 5: Continued.

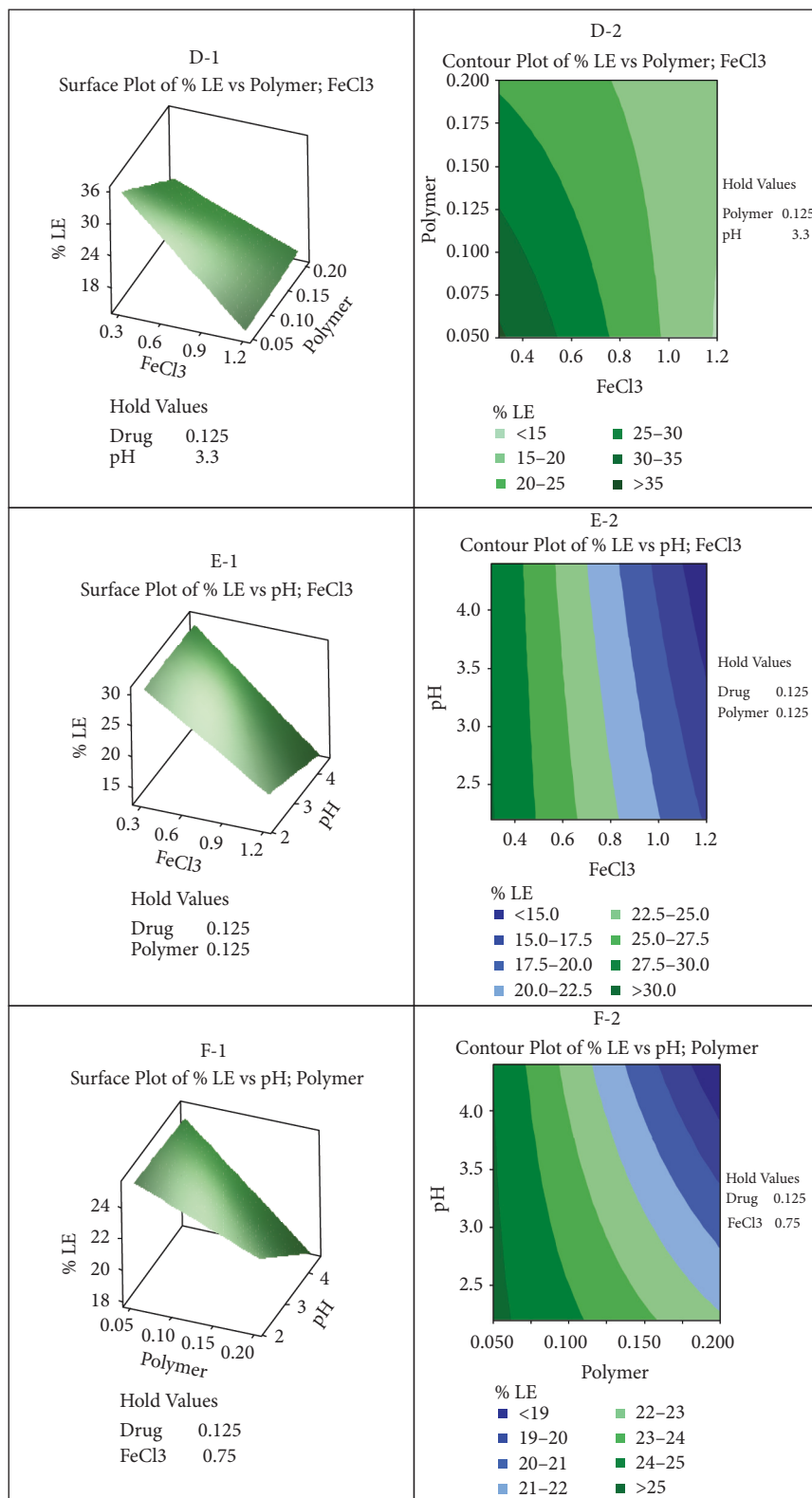


FIGURE 5: Contour and surface plots for %LE.

than 0.175 gm of drug and a low concentration of polymer at less than 0.1 gm, with a fixed pH (3.3) and FeCl_3 at 0.75 gm.

Figure 5(g) shows the surface plot of %LE, where the independent variables are polymer and FeCl_3 . From the figure, the highest %LE (>35%) can be collected at a low level of FeCl_3 (<0.8 gm) and a low level of polymer (<0.125 gm) with a fixed value of drug (0.125 gm) and pH at 3.3 gm. These results are also shown in the contour plot in Figure 5(h).

From Figure 5(i) of the surface plot and Figure 5(j) of the contour plot of %LE, the %LE with more than 30% can be collected at a low level of FeCl_3 (<0.6 gm) with a large range in pH starting from 2.2 to 4.4, with fixed values of drug (0.125 gm) and polymer (0.125 gm).

The effect of polymer and pH on the %LE is shown in Figures 5(k) and 5(l). The results show that a %LE greater than 25% can be collected by using a concentration less than 0.100 gm of polymer with a large range in pH starting from 2.2 to 4.4, with a fixed value of drug (0.125 gm) and FeCl_3 at 0.75 gm.

Figure 6(a) shows the surface plot of zeta potential, where the independent variables are drug and FeCl_3 . From the figure, the highest zeta potential (>25%) can be collected at a large scale of drug starting from 0.050 to 0.200 gm and a high level of FeCl_3 (>0.9 gm) with a fixed value of polymer (0.125 gm) and pH at (3.3 gm). These results are also shown in the contour plot in Figure 6(b).

From Figure 6(c) of the surface plot and Figure 6(d) of the contour plot of the zeta potential, a zeta potential greater than 30% can be collected at a high level of drug (>0.159 gm) with a pH less than 2.5, with a fixed value of FeCl_3 (0.75) and polymer (0.125).

The effect of the polymer and drug on the zeta potential is shown in Figures 6(e) and 6(f). The results show that a zeta potential greater than 15% can be collected by using a large-scale drug starting from 0.050 to 0.200 gm, and the average scale of the polymer starts from 0.100 to 0.200 gm with a fixed pH (3.3) and FeCl_3 at 0.75 gm.

Figure 6(g) shows the surface plot of the zeta potential, where the independent variables are the polymer and FeCl_3 . From the figure, the highest zeta potential (>30%) can be collected at a high level of FeCl_3 (>1.0 gm), and the large scale of the polymer starts from 0.05 to 0.200 gm with a fixed value of drug (0.125 gm) and pH at (3.3 gm). These results are also shown in the contour plot in Figure 6(h).

From Figure 6(i) of the surface plot and Figure 6(j) of the contour plot of the zeta potential, a zeta potential of more than 30% can be collected at a low level of FeCl_3 (<1.0 gm) with a large range in pH starting from 2.2 to 4.4, with fixed values of drug (0.125 gm) and polymer (0.125 gm).

The effect of the polymer and pH on the zeta potential is shown in Figures 6(k) and 6(l). The results show that a zeta potential greater than 30% can be collected by using large-scale polymers starting from 0.50 to 0.200 gm with a low pH (<2.5) and fixed values of drug (0.125 gm) and FeCl_3 (0.75 gm).

3.3.4. Main Effects Plot for %LE and Zeta Potential. The main effect plots are used to assess the significance of each variable at various levels, which are related to each other by line on the outcome or response.

From Figure 7(a), the %LE can reach 34% by using 0.18 gm of drug. In addition, the relation between the %LE and concentration of drug was direct. However, the relationships between %LE and FeCl_3 , polymer, and pH were indirect. According to the figure, we can collect 30%, 25%, and 22% LE by using 0.4 gm FeCl_3 , 0.06 gm polymer, and 2.2 PH, respectively.

From Figure 7(b), the zeta potential can reach 30% by using 1.2 g of FeCl_3 ; in addition, the relationship between the zeta potential and concentration of FeCl_3 was direct. However, the relationships between the zeta potential and the drug, polymer, and pH were indirect. According to the figure, we can collect 15%, 15%, and 30% zeta potentials by using 0.06 g of drug, 0.06 g of polymer, and 2.2 PH, respectively.

3.3.5. The Interaction between the Factor Effects on %LE and Zeta Potential. From Figure 8(a), the interaction between drug*PH indicates that, to prepare the nanocomposite with 32%, we should use 0.2 gm of drug at different pH values (2.2, 3.3, and 4.4). To prepare 40% LE, we used 0.2 gm of drug and 0.05 gm of polymer. In addition to preparing nanocomposites with 48% LE, we used 0.2 g of drug with 0.3 g of FeCl_3 .

Figure 8(a) also describes the interaction between FeCl_3 *PH and the FeCl_3 *polymer. Based on the figure, we can prepare a nanocomposite with 30% LE at 0.4 gm FeCl_3 and pH 2.2, whereas, to prepare a nanocomposite with 35% LE, we should use 0.41 gm FeCl_3 and 0.05 polymer.

Figure 8(a) also shows the interaction between polymer*PH and the effect on %LE. Based on the figure, we can prepare 20% LE in the nanocomposite by using 0.06 gm polymer and 2.2 PH media.

From Figure 8(b), the interaction between drug*PH indicates that, to prepare nanocomposites with 22%, we should use 0.2 gm of drug at different pH values (2.2). If the lines are parallel to the drug with FeCl_3 , the plot shows that there is no interaction between these two factors, and if the lines are parallel to the drug with polymer, the plot shows that there is no interaction between these two factors.

Figure 8(b) also describes the interaction between FeCl_3 *PH and the FeCl_3 *polymer. Based on the figure, we can prepare nanocomposites with 20% zeta potential at 1.2 gm FeCl_3 at different pH values (2.2, 3.3, and 4.4), whereas, to prepare nanocomposites with 30% zeta potential, we should use 1.2 gm FeCl_3 and 0.05 polymer.

Figure 8(b) also shows the interaction between polymer*PH and the effect on the zeta potential. Based on the figure, we can prepare a 30% zeta potential nanocomposite by using 0.2 mg polymer and 2.2 PH media.

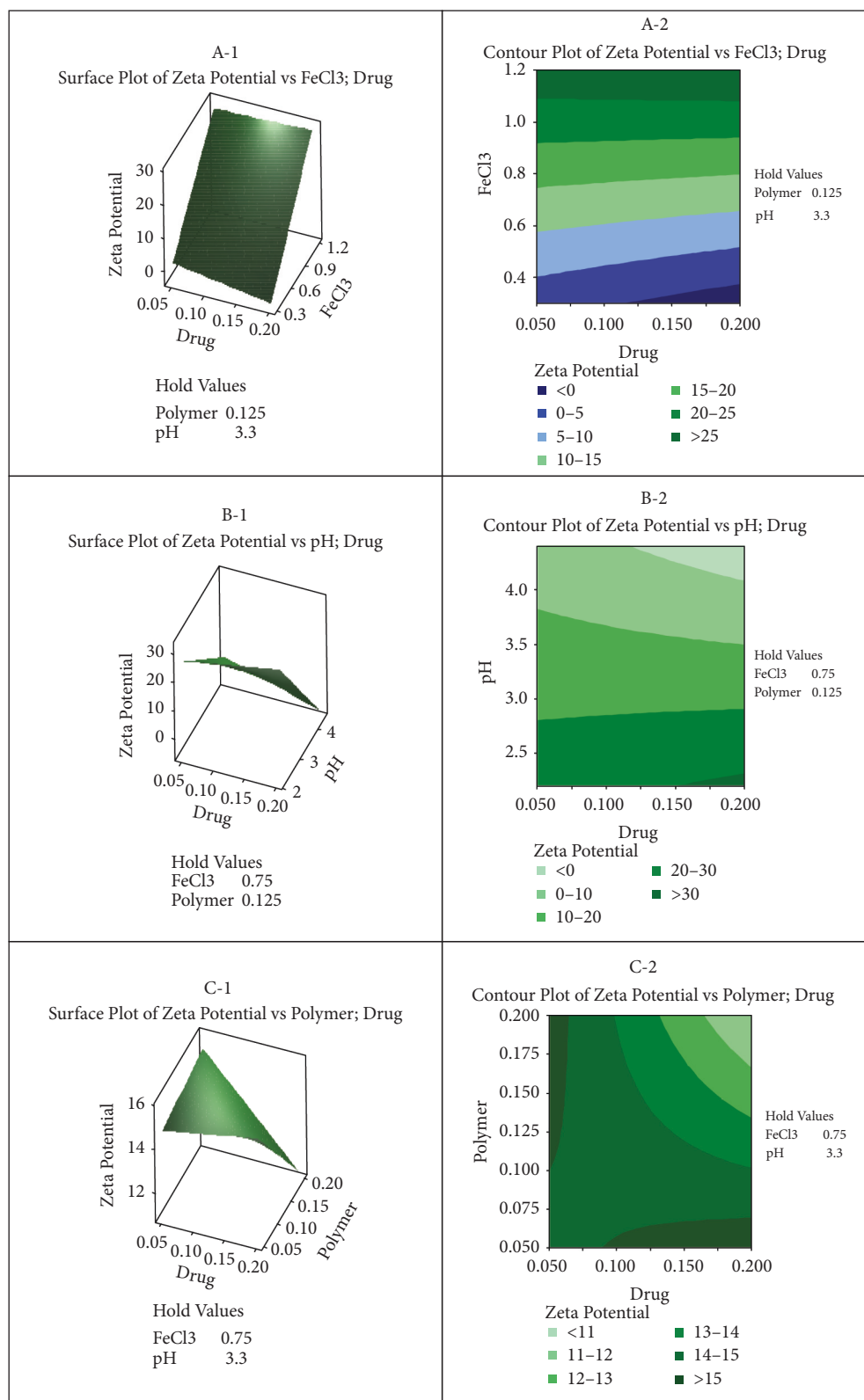


FIGURE 6: Continued.

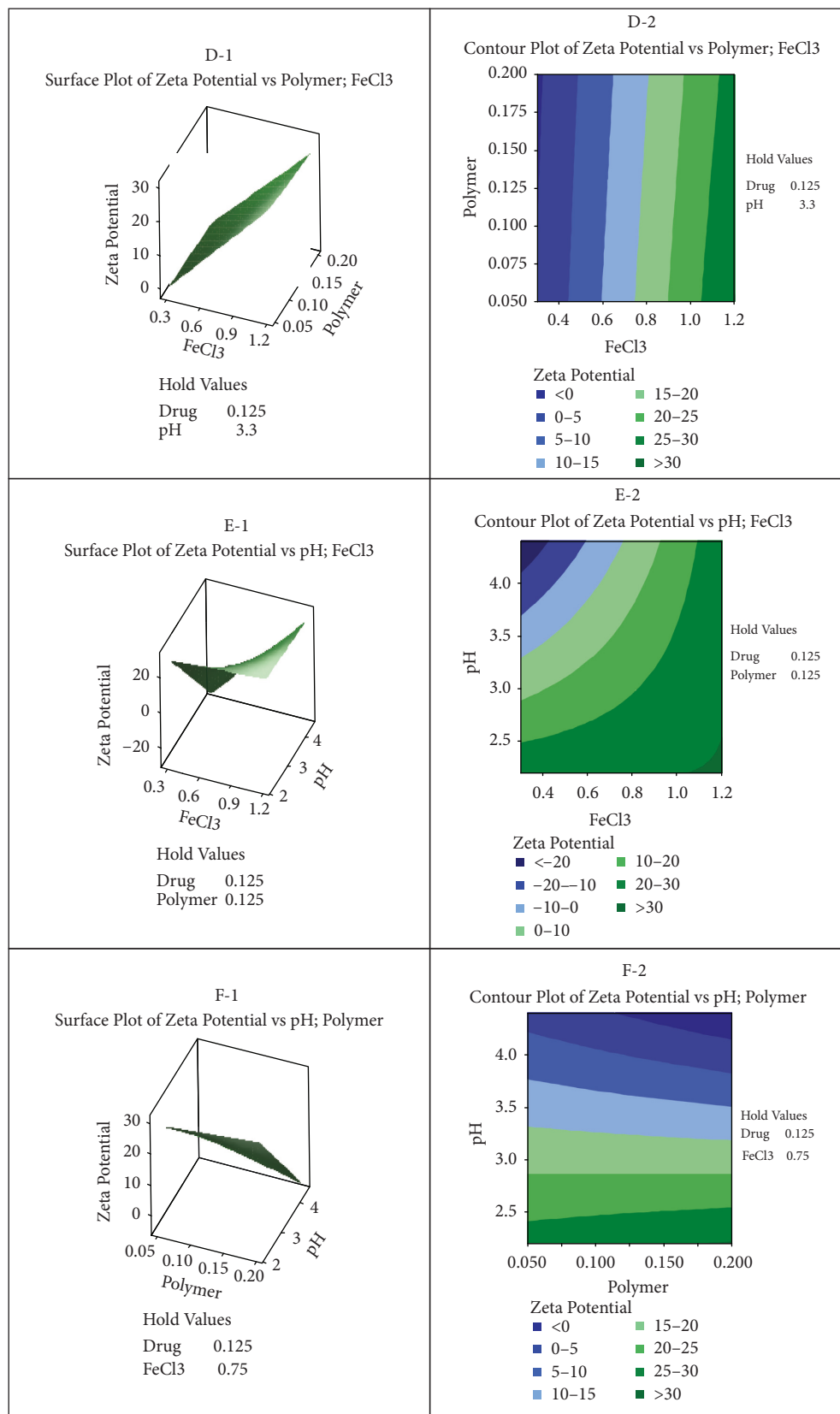


FIGURE 6: Contour and surface plots for zeta potential.

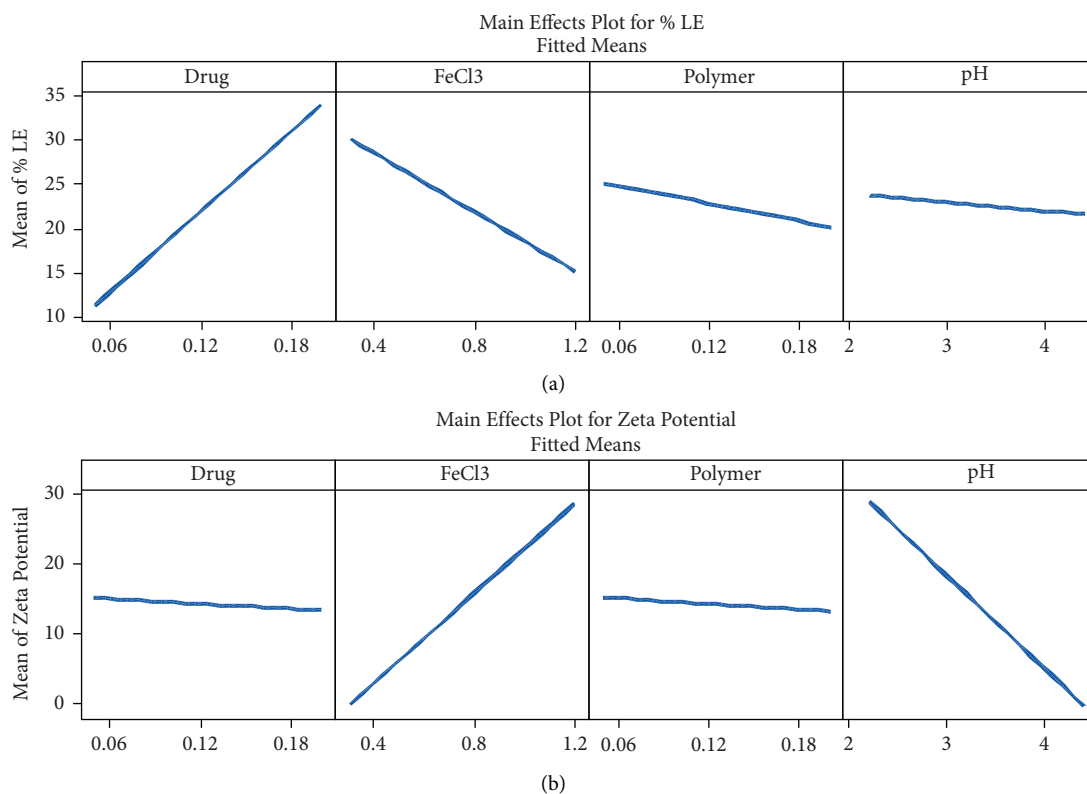


FIGURE 7: Main effects plot for %LE (a) and zeta potential (b).

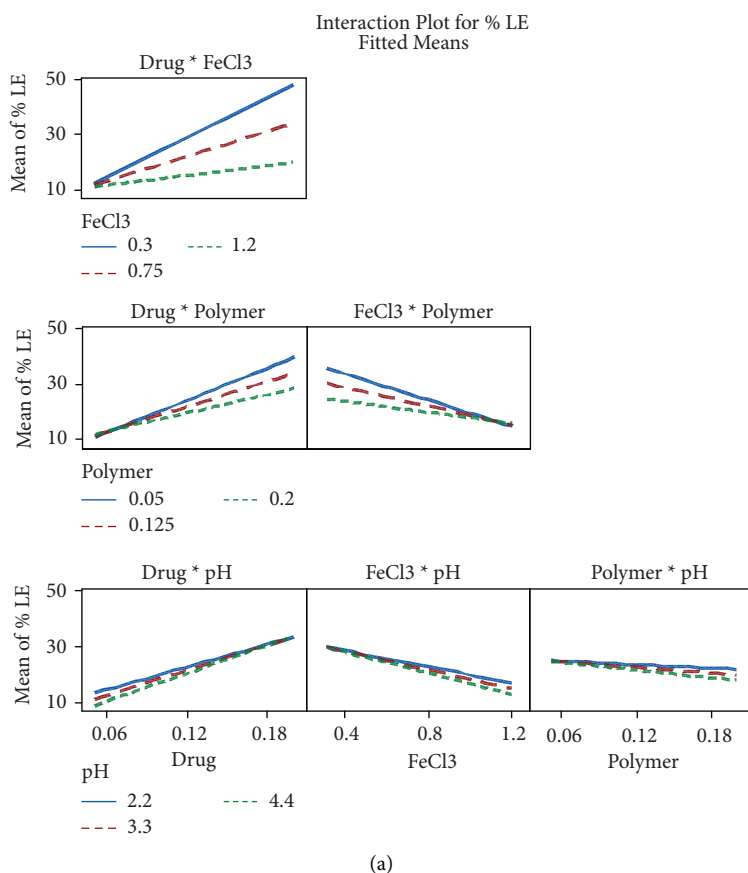


FIGURE 8: Continued.

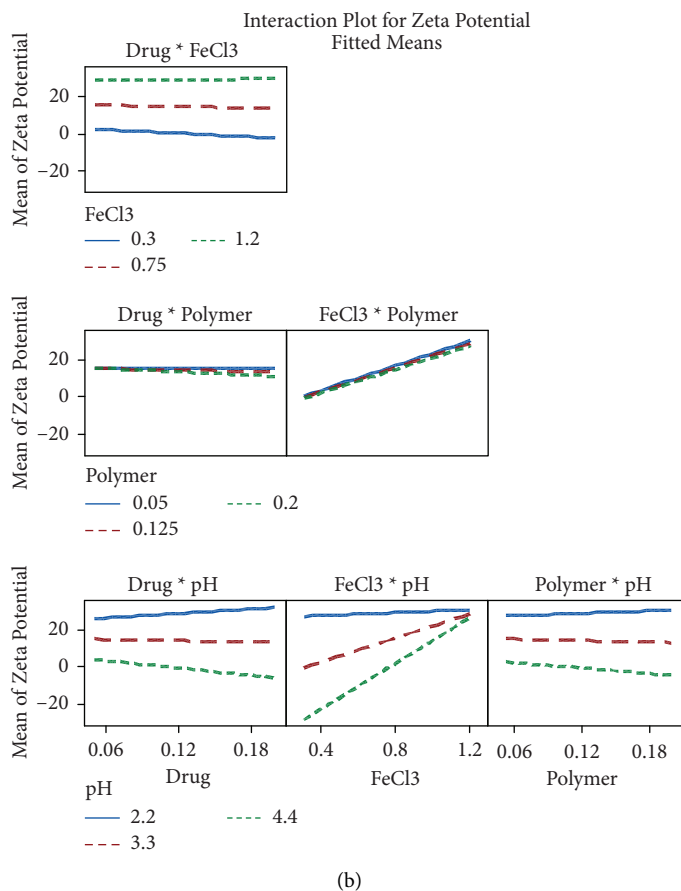


FIGURE 8: Interaction plot for LE% (a) and zeta potential (b).

3.4. Optimization and Validation of %LE and Zeta Potential

3.4.1. Optimization of %LE and Zeta Potential. Figure 9 shows an optimized concentration for the response factors %LE and zeta potential. The first optimized compound selected had the highest %LE and the highest Zeta potential.

The second and third optimized samples were collected randomly by changing the vertical red line in Figure 9.

3.4.2. Validation of %LE and Zeta Potential. According to the optimized nanocomposite, the other two samples in Figure 9 contain three independent variables with the predicate %LE and zeta potential. These three samples were prepared in the lab, and, after that, we deferred the %LE and zeta potential.

From Table 8, we can see that the bias for the first formula was approximately 5.3% and 14.6% (drug = 0.2, FeCl₃ = 0.3, polymer = 0.05, and pH = 2.2) for %LE and zeta potential, respectively. In addition, the bias for the second formula was approximately -5.2% and -13.1% for %LE and zeta potential, respectively (drug = 0.121, FeCl₃ = 0.6926, polymer = 0.12, and pH = 3.1) and the bias for the third formula was approximately -4.1% and -19.0% for %LE and zeta potential, respectively (drug = 0.2, FeCl₃ = 0.3, polymer = 0.2, and pH = 2.2). These findings and information supported the validity of the model created and indicated good correlation

between experimental and predicted values. A bias formula was developed under optimized factors to compare experimental values with the predictor values.

3.5. Characterizations of the Optimized Nanocomposite

3.5.1. X-Ray Diffraction (XRD). Powder XRD patterns of polymer nanoparticles and cromolyn-polymer nanocomposites are presented in Figures 10(a) and 10(b), respectively. From Figure 10(a), the strong peaks at $2\theta = 31.7^\circ$ and 45.3° indicate semicrystalline properties. In addition, the cromolyn-polymer nanocomposite in Figure 10(b) shows a peak similar to that of polymer nanoparticles. From the literature, free cromolyn shows different sharp peaks at 2θ 8, 9.8, 11.5, 14, 16.9, 19.7, 24.3, and 26.6, indicating that cromolyn is highly crystalline in nature [20].

In addition, the absence of characteristic drug peaks in the nanocomposite shown in Figure 1(b) indicated that the drug had converted from a crystalline into an amorphous form and was incorporated into the polymer.

3.5.2. Fourier Transform Infrared (FTIR) Spectroscopy. Figures 11(a)–11(d) show FTIR spectra for cromolyn, polymer, polymer nanoparticle, and nanocomposite, respectively. From the figures, pure cromolyn showed basic

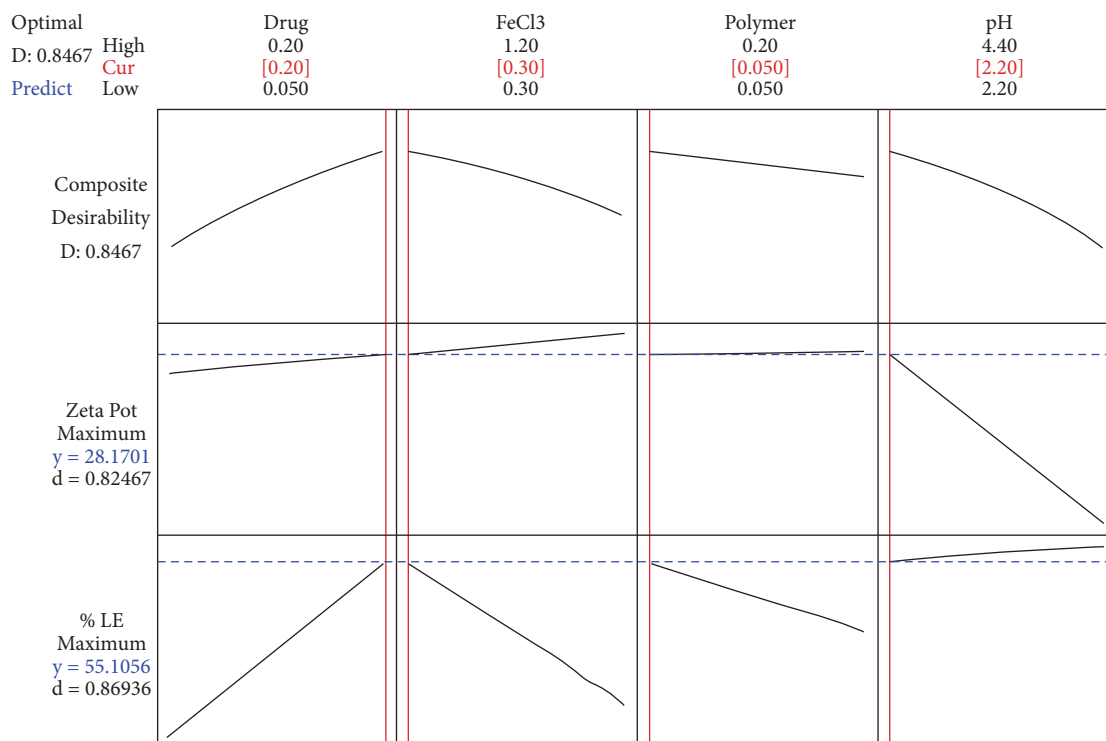


FIGURE 9: Response optimization plot for different responses.

TABLE 8: Comparative results between observed and predicted response values of variables of optimized formulation.

Concentrations	Experimental response	Predicted values	Observed values	Bias (%)
Drug (0.2 gm) FeCl ₃ (0.3 gm) Polymer (0.05 gm) pH = 2.2	LE (%)	55.1%	58.0%	5.3%
Drug (0.121 gm) FeCl ₃ (0.6926 gm) Polymer (0.121 gm) pH = 3.1	Zeta potential (mV)	28.1 mV	32.2 mV	14.6%
Drug (0.2 gm) FeCl ₃ (0.3 gm) Polymer (0.2 gm) pH = 2.2	LE (%)	23.2%	22.0%	-5.2%
	Zeta potential (mV)	15.3 mV	13.3 mV	-13.1%
	LE (%)	39.3%	37.7%	-4.1%
	Zeta potential (mV)	29.5 mV	23.9 mV	-19.0%

% bias was calculated as (observed value - predicted value/predicted value) × 100

peaks at 1605 cm^{-1} due to (C=O), a broad band at 3285 cm^{-1} due to (O-H) stretching vibrations, and characteristic peaks at 2880 cm^{-1} due to (C-H alkane). An aromatic C-H gives bands at 1477 cm^{-1} , 1573 cm^{-1} , and 1410 cm^{-1} (asymmetric and symmetric COO⁻) and a large number of characteristic absorption bands in the fingerprint region ($1400\text{--}600\text{ cm}^{-1}$) [21].

The IR spectra of the polymer are shown in Figure 11(b). The stretching vibrations of the carboxylic and carbonyl groups ranged from 1720 to 1727 cm^{-1} , and the formation of hydrogen bonding carboxylic acid O-H stretching appeared as a very broad band from 2543 to 3623 cm^{-1} . In the range of 3732 to 3737 cm^{-1} , a weak band for the monomeric O-H stretch band was also observed. From 1626 to 1636 cm^{-1} ,

strong bands of the stretching vibration for the carbonyl bond of the amide group were observed. The IR band of amide group NH bonds was observed for stretching and bending vibrations between 3268 and 3316 cm^{-1} and between 1517 and 1527 cm^{-1} , respectively [22].

The IR spectra of blank-polymer nanoparticles are shown in Figure 11(c). The spectrum of the polymer nanoparticles showed a characteristic vibrational peak for O-H at 3320 cm^{-1} . The peak observed at approximately 583 cm^{-1} is characteristic of Fe vibrations. Comparing the spectrum of the nanocomposite with the spectrum of the blank-polymer particle, specific peaks of cromolyn appeared at 1604 cm^{-1} due to C=O, and a band at approximately 1477 cm^{-1} was also observed due to aromatic C-H. All these

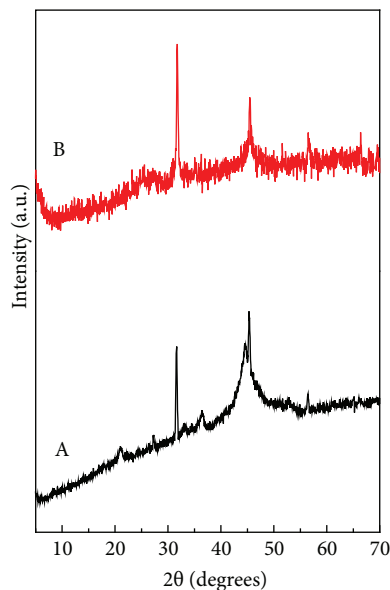


FIGURE 10: Powder X-ray diffraction patterns of the polymer nanoparticles (a) and cromolyn-polymer nanocomposite (b).

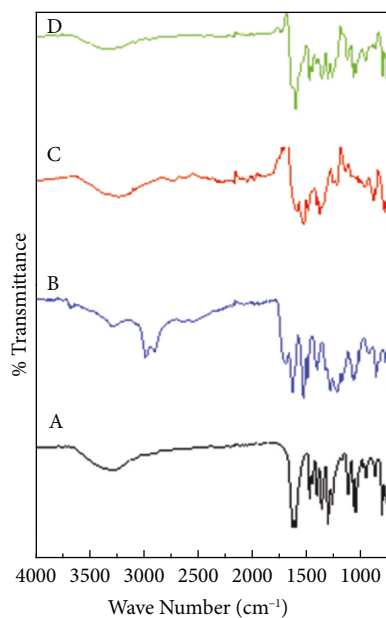


FIGURE 11: FTIR of the cromolyn (a), polymer (b), polymer nanoparticle (c), and nanocomposite (d).

results indicate the incorporation of cromolyn into the nanocomposite, as shown in Figure 11(d).

3.5.3. Scanning Electron Microscopy (SEM). The surface morphology of the samples for polymer nanoparticles and nanocomposites as studied by scanning electron microscopy (FE-SEM) is shown in Figures 12(a) and 12(b), respectively. Figure 12 shows a spherical shape and nearly uniform size with diameters of 55 and 68 nm for the polymer nanoparticles and nanocomposites, respectively.

3.5.4. In Vitro Release Study. The in vitro release of cromolyn from the cromolyn-polymer nanocomposite at pH 7.4 is shown in Figure 13. It is shown that the amount of cromolyn released at 23 hours was 100%. Cromolyn is released via several mechanisms, such as diffusion, erosion, and swelling. In the diffusion method, the drug diffuses from the matrix of the polymer to the surrounding area. In the erosion method, the polymer breaks the bond and then releases the drug.

The medium's pH value, surrounding media enzymes, and uptake of water via the polymer can all affect drug

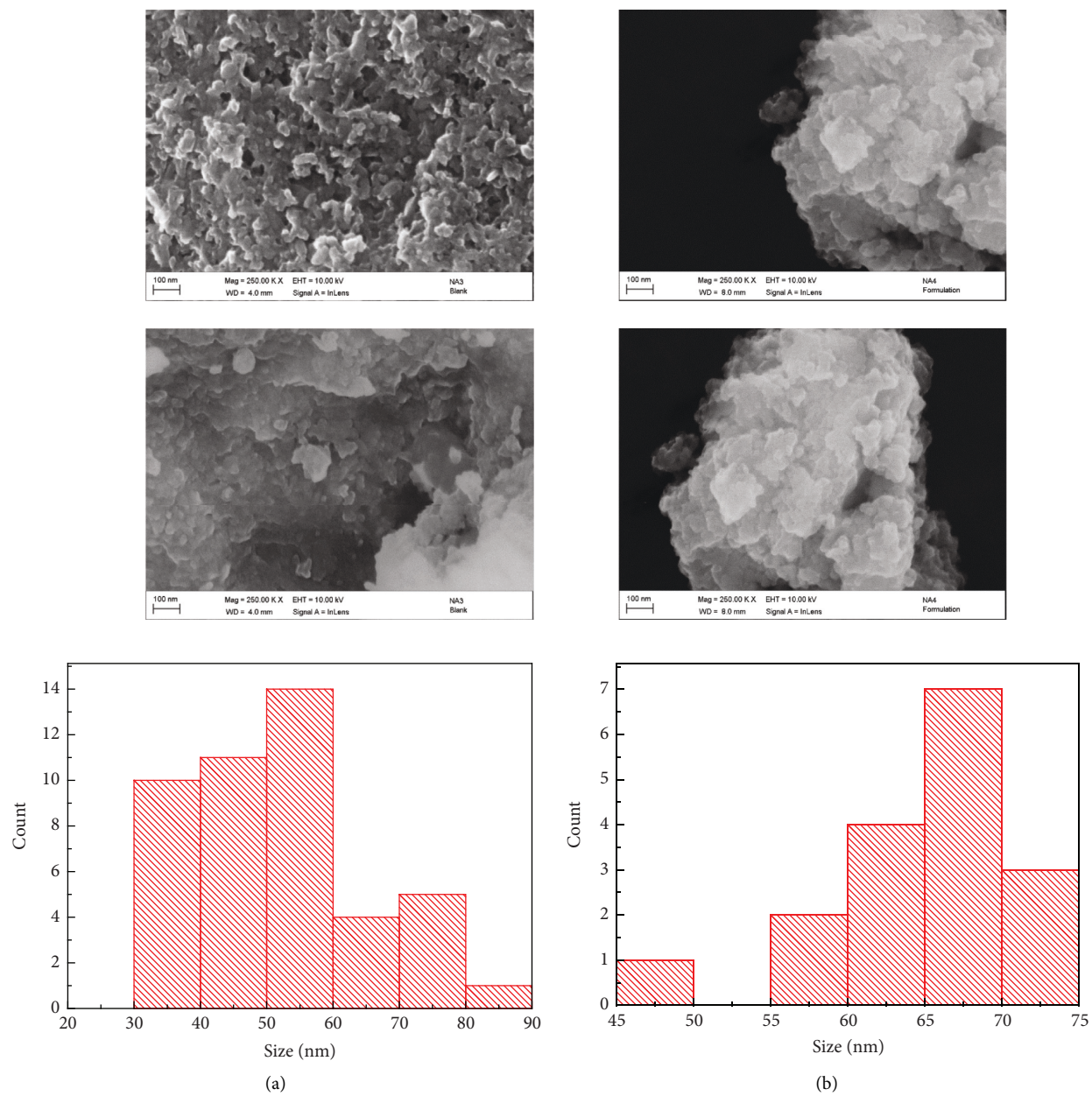


FIGURE 12: Scanning electron microscope images of polymer nanoparticles (a) and polymer nanocomposites (b).

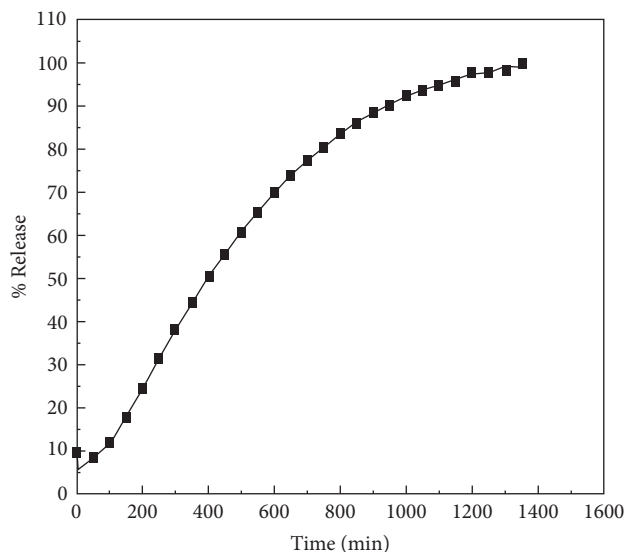


FIGURE 13: In vitro release profile of cromolyn from the cromolyn-polymer nanocomposite.

release. The swelling of hydrogel beads is one of the main mechanisms that play an important role in drug release by allowing water to enter through the polymer and dissolve it.

4. Conclusion

In this study, the main aim was to use polyamide-disulfide nanoparticles as a drug delivery system. We used cromolyn as a model and formed nanocomposites. In this work, we investigated the effect of independent variables (cromolyn, FeCl_3 , polymer, and pH) on the dependent variable (%LE, zeta potential, and particle size). We used Minitab 18 software to evaluate the nanocomposite. The study obtained %LE (25%–45%) and zeta potential (15%–30%). The formulation that we prepared can be used as a drug delivery system for cromolyn to improve its absorption, stability, bioavailability, and drug release profile for extended release for 23 hours. This study indicated that cromolyn with the polymer had the most significant impact on %LE and zeta potential.

Data Availability

The data are available upon request from Professor Samer Hasan Ahmad Hussein-Al-Ali (e-mail: sameralali72@yahoo.com or samer.alali@iu.edu.jo).

Conflicts of Interest

The authors report that there are no conflicts of interest in this work.

Acknowledgments

The authors would like to thank the Faculty of Pharmacy at Isra University for providing funding for this research under grant no. 2020/2021/4–23. Also, the authors would like to acknowledge the Institute of Functional Nanosystems for the

permission to use their advanced facilities in UIM University (Germany).

References

- [1] A. Cappy, D. Stievenard, and D. Vuillaume, "Nanotechnology: the next industrial revolution?" in *Gallium Arsenide Applications Symposium*, pp. 1–4, 2002.
- [2] S. A. Agnihotri, N. N. Mallikarjuna, and T. M. Aminabhavi, "Recent advances on chitosan-based micro- and nanoparticles in drug delivery," *Journal of Controlled Release*, vol. 100, no. 1, pp. 5–28, 2004.
- [3] T. Yih and M. Al-Fandi, "Engineered nanoparticles as precise drug delivery systems," *Journal of Cellular Biochemistry*, vol. 97, no. 6, pp. 1184–1190, 2006.
- [4] S. Gelperina, K. Kisich, M. D. Iseman, and L. Heifets, "The potential advantages of nanoparticle drug delivery systems in chemotherapy of tuberculosis," *American Journal of Respiratory and Critical Care Medicine*, vol. 172, no. 12, pp. 1487–1490, 2005.
- [5] S.-D. Li and L. Huang, "Pharmacokinetics and biodistribution of nanoparticles," *Molecular Pharmaceutics*, vol. 5, no. 4, pp. 496–504, 2008.
- [6] D. K. Ali, A. M. Al-Zuheiri, and B. A. Sweileh, "pH and reduction sensitive bio-based polyamides derived from renewable dicarboxylic acid monomers and cystine amino acid," *International Journal of Polymer Analysis and Characterization*, vol. 22, no. 4, pp. 361–373, 2017.
- [7] S. Murphy, "Cromolyn sodium: basic mechanisms and clinical usage," *Pediatric Asthma, Allergy and Immunology*, vol. 2, no. 4, pp. 237–254, 1988.
- [8] S. Yasmeen, S. Khatun, F. A. Qais, and F. Abul Qais, "Characterization of interactions between cromolyn sodium and bovine serum albumin by spectroscopic, calorimetric and computational methods," *Journal of Biomolecular Structure and Dynamics*, vol. 38, no. 3, pp. 722–732, 2019.
- [9] A. W. G. Alani and J. R. Robinson, "Mechanistic understanding of oral drug absorption enhancement of cromolyn sodium by an amino acid derivative," *Pharmaceutical Research*, vol. 25, no. 1, pp. 48–54, 2008.
- [10] R. N. Brogden, T. M. Speight, and G. S. Avery, "Sodium cromoglycate (cromolyn sodium): a review of its mode of action, pharmacology, therapeutic efficacy and use," *Drugs*, vol. 7, no. 3, pp. 164–282, 1974.
- [11] W. B. Liechty, D. R. Kryscio, B. V. Slaughter, and N. A. Peppas, "Polymers for drug delivery systems," *Annual Review of Chemical and Biomolecular Engineering*, vol. 1, pp. 149–173, 2010.
- [12] I. Rodriguez, J. Flores Bello, J. Marie Serrano Valcarcel, and V. Lopez-Mejias, "Design of potential pharmaceutical-based metal complexes derived from cromolyn a mast cell stabilizer," *ACS Omega*, vol. 5, no. 46, pp. 29714–29721, 2020.
- [13] P. Sacco, S. Pedroso-Santana, Y. Kumar, N. Joly, P. Martin, and P. Bocchetta, "Ionotropic gelation of chitosan flat structures and potential applications," *Molecules*, vol. 26, no. 3, p. 660, 2021.
- [14] S. Pedroso-Santana and N. Fleitas-Salazar, "Ionotropic gelation method in the synthesis of nanoparticles/microparticles for biomedical purposes," *Polymer International*, vol. 69, no. 5, pp. 443–447, 2020.
- [15] H. A. K. Sabbagh, S. H. Hussein-Al-Ali, M. Z. Hussein, Z. Abudayeh, R. Ayoub, and S. M. Abudoleh, "A statistical study on the development of metronidazole-chitosan-alginate

- nanocomposite formulation using the full factorial design,” *Polymers*, vol. 12, no. 4, p. 772, 2020.
- [16] I. Kuncahyo, S. Choiri, A. Fudholi, R. Martien, and A. Rohman, “Assessment of fractional factorial design for the selection and screening of appropriate components of a self-nanoemulsifying drug delivery system formulation,” *Advanced Pharmaceutical Bulletin*, vol. 9, no. 4, pp. 609–618, 2019.
- [17] N. Subramanian, A. Yajnik, and R. S. R. Murthy, “Artificial neural network as an alternative to multiple regression analysis in optimizing formulation parameters of cytarabine liposomes,” *AAPS PharmSciTech*, vol. 5, no. 1, pp. 11–19, 2004.
- [18] S. H. Hussein-Al-Ali, S. M. Abudoleh, Q. I. A. Abualassal, Z. Abudayeh, Y. Aldalahmah, and M. Z. Hussein, “Preparation and characterisation of ciprofloxacin-loaded silver nanoparticles for drug delivery,” *IET Nanobiotechnology*, vol. 16, no. 3, pp. 92–101, 2022.
- [19] S. H. Hussein-Al-Ali, M. Zobir, R. Ayoub, S. Fakurazi, Q. Abualassal, and Y. Al-Dalahmeh, “Development of new drug formulations: cetirizine-polymers nanoparticles,” *Acta Poloniae Pharmaceutica—Drug Research*, vol. 78, no. 3, pp. 385–398, 2021.
- [20] R. R. Patel, G. Khan, S. Chaurasia, N. Kumar, and B. Mishra, “Rationally developed core-shell polymeric-lipid hybrid nanoparticles as a delivery vehicle for cromolyn sodium: implications of lipid envelop on in vitro and in vivo behaviour of nanoparticles upon oral administration,” *RSC Advances*, vol. 5, no. 93, pp. 76491–76506, 2015.
- [21] R. R. Patel, S. Chaurasia, G. Khan, P. Chaubey, N. Kumar, and B. Mishra, “Cromolyn sodium encapsulated PLGA nanoparticles: an attempt to improve intestinal permeation,” *International Journal of Biological Macromolecules*, vol. 83, pp. 249–258, 2016.
- [22] G. Lawrie, I. Keen, B. Drew et al., “Interactions between alginate and chitosan biopolymers characterized using FTIR and XPS,” *Biomacromolecules*, vol. 8, no. 8, pp. 2533–2541, 2007.